American Mineralogist, Volume 110, pages 1527–1537, 2025

Moxuanxueite, $NaCa_6Zr(Si_2O_7)_2OF_3$, a new wöhlerite-group mineral from Gejiu alkaline complex, Yunnan Province, China

Kai Qu[1,2,3,*,†], Guochen Dong[1,*], Ting Li[4], Guang Fan[4], Xiangping Gu[5,‡], Yufei Wang[1], and Yanjuan Wang[1,6,§]

[1]School of Earth Sciences and Resources, China University of Geosciences (Beijing), Beijing 100083, China
[2]Tianjin Center, China Geological Survey, Tianjin 300170, China
[3]School of Earth Sciences and Engineering, Nanjing University, Nanjing 210023, China
[4]Beijing Research Institute of Uranium Geology, Beijing 100029, China
[5]School of Geosciences and Info-Physics, Central South University, Changsha 410012, Hunan, China
[6]Department of Geosciences, University of Padova, Padova 35131, Italy

Abstract

Moxuanxueite, ideally $NaCa_6Zr(Si_2O_7)_2OF_3$, is a new wöhlerite-group mineral from the Gejiu alkaline complex, Yunnan Province, China. This new species occurs as subhedral to euhedral polysynthetic twinned grains, and as elongate crystals up to 1 mm in size, commonly coexisting with tiny baddeleyite at the grain margins and usually associated with calcioancylite-(La), bobtraillite, catapleiite, fluorite, and jadeite. Moxuanxueite is light yellow in color with a metallic luster. It is very brittle with conchoidal fracture and has a calculated density of 3.231 g/cm^3. The empirical formula calculated on the basis of O + F = 18 apfu is $Na_{1.38}Ca_{5.21}Fe_{0.23}Mn_{0.22}(Zr_{0.88}Ti_{0.14})_{\Sigma 1.02}(Si_{2.01}O_7)_2(F_{3.15}O_{0.85})_{\Sigma 4.00}$. The ideal formula requires (wt%) Na_2O 4.06, CaO 44.04, ZrO_2 16.13, SiO_2 31.46, F 7.46, O≡F –3.14, and a total of 100 wt%. The mineral is triclinic, with space group $P\bar{1}$ (#2), a = 11.0235(3) Å, b = 10.9641(4) Å, c = 7.3805(4) Å, α = 109.523(2)°, β = 109.881(2)°, γ = 83.434(2)°, V = 790.63(6) Å^3, and Z = 2. The seven strongest X-ray powder diffraction lines [d in Å (I) (hkl)] are: 3.005 (100) ($\bar{1}12$), 2.870 (57) (230), 1.849 (32) ($\bar{2}\,\bar{2}4$), 10.42 (30) ($\bar{1}00$), 2.496 (26) ($1\bar{4}0$), 3.280 (23) ($\bar{3}\,\bar{1}0$), and 1.701 (20) ($1\bar{6}2$). Moxuanxueite is isostructural with hiortdahlite [$Na_2Ca_4(Zr_{0.5}Ca_{0.5})(Si_2O_7)_2OF_3$], and the transformation between the two phases is via the substitution mechanism: $2Ca^{2+} \leftrightharpoons Na^+ + 0.5Zr^{4+} + 0.5Ca^{2+}$. The new mineral is named in honor of Xuanxue Mo (b. 1938), a distinguished petrologist from the China University of Geosciences (Beijing), for his outstanding contribution to magmatism and related mineralization in China.

Keywords: Moxuanxueite, wöhlerite group, new mineral, Gejiu alkaline complex, feldspathoid syenite

Introduction

Wöhlerite-group minerals (also called the "cuspidine group" in some earlier literature) are typical accessory Zr-Ti-Nb-bearing disilicates with monoclinic or triclinic symmetry found in agpaitic rocks from localities worldwide and are considered an important carrier for high field strength elements (HFSE) in carbonatites and agpaitic feldspathoid syenites (Mariano and Roeder 1989; Chakhmouradian and Williams 2004; Chakhmouradian 2006; Schmidt et al. 2023). The general formula of wöhlerite-group mineral is $X_8(Si_2O_7)_2W_4$, where X = Na^+, Ca^{2+}, Mn^{2+}, Fe^{2+}, Ti^{4+}, Zr^{4+}, and Nb^{5+}; and W = F^-, OH^-, and O^{2-} (Dal Bo et al. 2022). Up to now, 12 minerals belonging to the wöhlerite group have been approved by the Commission on New Minerals, Nomenclature and Classification (CNMNC) of the International Mineralogical Association (IMA) (Table 1). The crystal structure of wöhlerite-group minerals can be characterized by four-column-wide octahedral walls, interconnected by corner-sharing and through the Si_2O_7 groups (Merlino and Perchiazzi 1988; Fig. 1). Previous studies show that there are four distinct types of unit cells in wöhlerite-group minerals, including 10 distinct patterns to make the disilicate groups connect to the octahedral framework (Merlino and Perchiazzi 1988; Biagioni et al. 2012). Among these, hiortdahlite and moxuanxueite with triclinic symmetry are characterized by two cationic walls in the unit cell and distinguished from other monoclinic wöhlerite-group minerals (Dal Bo et al. 2022). It is worth noting that an unambiguous phase identification, either from chemical composition or X-ray powder diffraction analysis, is difficult owing to the presence of multiple homo- and heterovalent substitutions in wöhlerite-group minerals (Sharygin et al. 1996a; Bellezza et al. 2004).

Moxuanxueite was found in the Gejiu alkaline complex, Yunnan Province, China. The new mineral, its name and symbol (Mox) have been approved by the Commission on New Minerals, Nomenclature and Classification of the International Mineralogical Association (IMA-CNMNC). It is named in honor of Xuanxue Mo (Fig. 2), born in 1938, a distinguished petrologist at the China University of Geosciences (Beijing), for his outstanding

* Co-corresponding author E-mails: qukai_tcgs@foxmail.com Orcid https://orcid.org/0000-0002-4961-9598, donggc@cugb.edu.cn

‡ Orcid https://orcid.org/0000-0001-5278-6656
§ Orcid https://orcid.org/0000-0002-6985-2012

Table 1. Ideal formulas and unit-cell parameters for the wöhlerite group minerals

Mineral	Symbol[a]	Ideal end-member formula[b]	Crystal system	Space group	Z	Unit-cell parameters (Å, °)						Ref.
						a	*b*	*c*	α	β	γ	
Wöhlerite	Wöh	$Na_2Ca_4ZrNb(Si_2O_7)_2O_3F$	Mon.	$P2_1$	2	10.823	10.244	7.290	90	109.00	90	[1]
Niocalite	Nio	$Ca_7Nb(Si_2O_7)_2O_3F$	Mon.	*Pa*	2	10.863	10.431	7.370	90	110.1	90	[2]
Janhaugite	Jhg	$Na_3Mn_3Ti_2(Si_2O_7)_2(OH)_2OF$	Mon.	$P2_1/n$	4	10.668	9.787	13.931	90	107.82	90	[3]
Burpalite	Brp	$Na_4Ca_2Zr_2(Si_2O_7)_2F_4$	Mon.	$P2_1/a$	2	10.1173	10.4446	7.2555	90	90.039	90	[4]
Baghdadite	Bgd	$Ca_6Zr_2(Si_2O_7)_2O_4$	Mon.	$P2_1/a$	2	10.42	10.16	7.36	90	91.1	90	[5]
Cuspidine	Csp	$Ca_8(Si_2O_7)_2F_4$	Mon.	$P2_1/a$	2	10.919	10.485	7.485	90	109.55	90	[6]
Låvenite	Låv	$Na_2Ca_2Mn_2Zr_2(Si_2O_7)_2O_2F_2$	Mon.	$P2_1/a$	2	10.83	9.98	7.174	90	108.1	90	[7]
Normandite	Nmd	$Na_2Ca_2Mn_2Ti_2(Si_2O_7)_2O_2F_2$	Mon.	$P2_1/a$	2	10.828	9.790	7.054	90	108.20	90	[8]
Madeiraite	Mde	$Na_2Ca_2Fe_2Zr_2(Si_2O_7)_2O_2F_2$	Mon.	$P2_1/a$	2	10.880	10.0442	7.2250	90	108.78	90	[9]
Pilanesbergite	Pbt	$Na_2Ca_2Fe_2Ti_2(Si_2O_7)_2O_2F_2$	Mon.	$P2_1/a$	2	10.7811	9.7836	7.0348	90	108.072	90	[10]
Hiortdahlite	Hio	$Na_2Ca_4(Ca_{0.5}Zr_{0.5})Zr(Si_2O_7)_2OF_3$	Tric.	$P\bar{1}$	2	10.9517	10.9251	7.3550	109.369	109.180	83.873	[11]
Moxuanxueite	Mox	$NaCa_6Zr(Si_2O_7)_2OF_3$	Tric.	$P\bar{1}$	2	11.0235	10.9641	7.3805	109.523	109.881	83.434	[12]

Notes: References: [1] Mellini and Merlino (1979); [2] Mellini (1982); [3] Raade and Mladeck (1983); [4] Merlino et al. (1990); [5] Al-Hermezi et al. (1986); [6] Saburi et al. (1977); [7] Mellini (1981); [8] Chao and Gault (1997); [9] Mills et al. (2022); [10] Dal Bo et al. (2024); [11] Dal Bo et al. (2022); [12] this work.
[a] Mineral symbols are quoted from Warr (2021).
[b] The charge-balance ideal end-member formulas are given in the nomenclature of wöhlerite-group minerals (Dal Bo et al. 2022).

contribution to magmatism and related mineralization in China. The type material is deposited at the Geological Museum of China with the number M16103 (Xicheng district, Beijing, China).

Geological Setting

The Gejiu area is located in the western margin of the Cathaysia block (Du et al. 2009; Zhang et al. 2013) (Fig. 3a), which is adjacent to the southwestern part of the Lanping-Simao block separated by the Ailaoshan- Honghe Fault (Cheng et al. 2008; Zhang et al. 2013). The area is also situated in the southern region of the giant rift-Panxi rift, which extends almost N-S along the western border of the Yangtze craton (Zhao et al. 2012). The main strata in the area are Triassic sandstone and carbonates with basalt interlayers (Huang et al. 2016; Wang et al. 2019; Zhang et al. 2013). The crosscutting faults in the region are mainly W–E or NNE–SSW oriented and some folds are also associated with them (Wang 2006; Cheng et al. 2009; Zhang et al. 2013; Huang et al. 2016; Wang et al. 2019). Intense Mesozoic magmatism developed in the region, as represented by the occurrence of gabbro, monzonite, granite, and nepheline syenite (Yu 1993; Chen et al. 2013; Zhao et al. 2015) (Fig. 3b). The nepheline syenites are mainly divided into early-formed silica-saturated alkali syenites from the northeastern Baiyunshan intrusion and later-formed silica-undersaturated feldspathoid syenites from the northern Changlinggang intrusion (Wang et al. 2023a). All these rocks formed between 77.2–85.0 Ma with a peak at 82–84 Ma (Cheng et al. 2008; Cheng and Mao 2010; Cheng 2012; Zhang 2013; Shang 2017; Chen 2019).

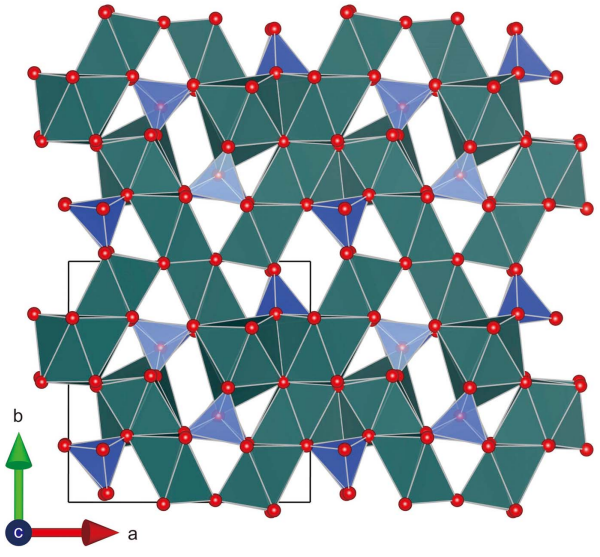

Figure 1. General view of the structure of the wöhlerite-group minerals.

Occurrence, Paragenesis, and Physical Properties

The new mineral, moxuanxueite, occurs within feldspathoid syenite (Fig. 3c) from the Changlinggang intrusion (23° 29′ 40″ N, 103° 4′ 41″ E), associated with albite, orthoclase, sodalite, jadeite, calcite, fluorite, ilmenite, magnetite, as well as other Zr- and REE-bearing minerals [such as baddeleyite, catapleiite, bobtraillite, eudialyte, britholite-(Ce), calcioancylite-(La), and calcioancylite-(Ce)] (Fig. 4). Moxuanxueite is a primary mineral disseminated in the groundmass, occurs as subhedral to euhedral polysynthetic twinned grains, and as elongate crystals up to 1 mm in size, and is commonly associated with tiny baddeleyite at the grain margins (Fig. 4b). Some pseudomorphs of primary

Figure 2. Photo of mineral namesake Xuanxue Mo (fieldwork in Yunnan Province, 2009). Provided by Xuanxue Mo.

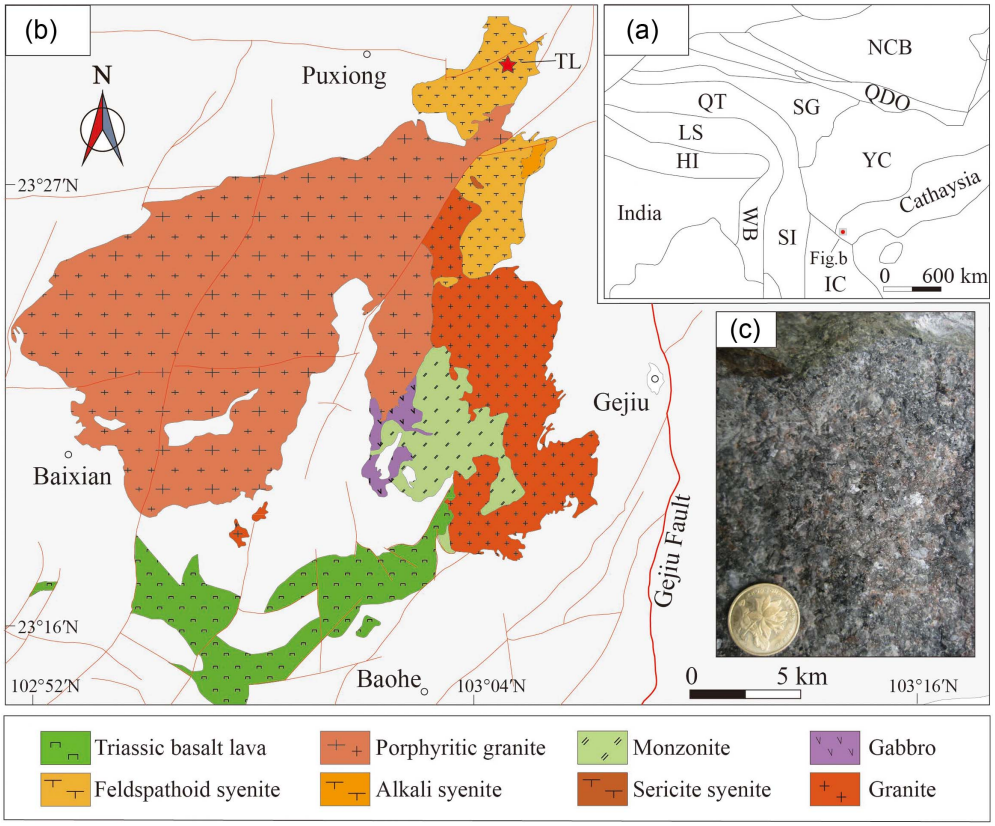

Figure 3. (**a**) Simplified tectonic map of eastern Asia (modified from Cheng et al. 2013); (**b**) geological map of the Gejiu, Yunnan (modified from Chen 2019; Wang et al. 2019, 2021); (**c**) outcrop of Changlinggang intrusions, where the type material (hand specimen No. 18CL-18) was collected. NCB = North China Craton; YC = Yangze Craton; QDO = Qinling-Dabie Orogen; Hi = Himalaya; WB = West Burma; LS = Lhasa; QT = Qiangtang; SI = Sibumasu Block; IC = Indo-China Block; SG = Songpan-Ganze Accretionary Complex; TL = Type Locality for moxuanxueite.

moxuanxueite tend to form in assemblages with various alteration minerals including: calcioancylite-(La), bobtraillite, catapleiite, fluorite, and jadeite (Wang et al. 2023a, 2023b). Moxuanxueite is light yellow to yellow-brown in hand specimen and colorless in the thin section, and it is translucent to transparent with vitreous luster and a white streak. The mineral is very brittle, with a distinct cleavage on {110}. The Mohs hardness is ~5½, and the mean micro-indentation hardness is VHN_{50} = 505 kg/mm^2 (range from 490 to 515 kg/mm^2). The density of 3.231 g/cm^3 is calculated based on the empirical formula and unit-cell volume refined from single-crystal X-ray diffraction (XRD) data. Optically, moxuanxueite is biaxial (+), with α = 1.636, β = 1.644, γ = 1.654. $2V$ (meas) = 83(3)°, $2V$ (calc) = 84°. The calculated compatibility ($1 - K_P/K_C$) is superior (–0.009) (Mandarino 1981).

Methods and Results

Infrared spectroscopy

An infrared spectrum of moxuanxueite was obtained in the range 4000–500 cm^{-1} using a Bruker LUMOS spectrometer with the ATR model at Beijing Research Institute of Uranium Geology. The infrared spectrum shows strong bands from 600 to 1100 cm^{-1} (Fig. 5), which can be compared to those of other members of the wöhlerite group, e.g., hiortdahlite from Langesundsfjord, Norway (Chukanov 2014), and normandite from Partomchorr Deposit, Russia (Frost et al. 2015). The bands at 1067, 1050, 928, 904, and 850 cm^{-1} are attributed to the Si-O stretching vibrations. The stretching vibrations of C–H bonds occurring at 2925 and 2855 cm^{-1} are due to organic compounds adsorbed on the thin section surface. No obvious peaks in the O-H stretching vibrations are present, which were observed in the 3650–3550 cm^{-1} range for other hydroxyl-bearing zirconium diorthosilicate minerals, for instance, dovyrenite (Galuskin et al. 2007).

Raman spectroscopy

A Raman spectrum of moxuanxueite over the 200 to 1100 cm^{-1} spectral range is shown in Figure 6. The spectrum was collected using a Renishaw in via micro-Raman system with a laser with a frequency of 532 nm (power: 4 mW, spatial resolution: 1 μm) and equipped with a motorized *x-y* stage and a Leica microscope with a 50× objective (Tianjin Center, China Geological Survey, China). The backscattered Raman signal was calibrated using a silicon plate, and the spectra were obtained from the polished thin section. In general, the most intense line at 948 cm^{-1} and the shoulder at 913 cm^{-1} are attributed to symmetric Si-O stretching vibrations within the Si_2O_7 groups, while the weaker peak at 1049 cm^{-1} probably corresponds to other internal tetrahedral modes. The strong peak at 664 cm^{-1} and its shoulder at 640 cm^{-1} are assigned to bending vibrations in Si_2O_7 groups (Sharygin et al. 1996a, 1996b). The bands at 582, 547, and 442 cm^{-1} are assigned to the O-Si-O

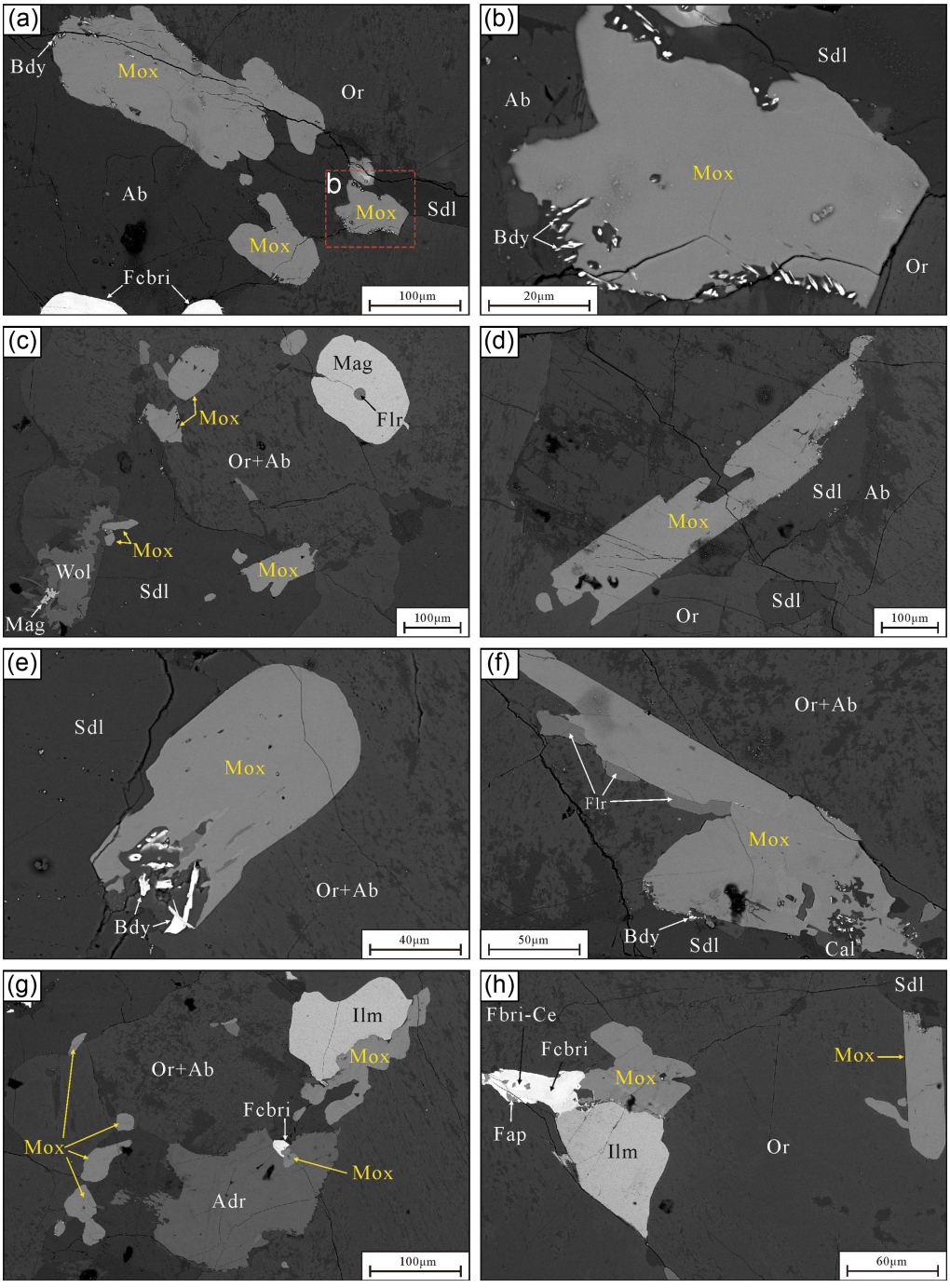

Figure 4. Backscatter electron (BSE) images of moxuanxueite and associated minerals. Mineral symbols (Warr 2021): Ab = albite; Adr = andradite; Bdy = baddeleyite; Cal = calcite; Fap = fluorapatite; Fbri-Ce = fluorbritholite-(Ce); Fcbri = fluorcalciobritholite; Flr = fluorite; Ilm = ilmenite; Mag = magnetite; Mox = moxuanxueite; Or = orthoclase; Sdl = sodalite; Wol = wollastonite.

bending vibrations (Frost et al. 2015). Bands below 320 cm^{-1} are attributed to lattice vibrations.

Chemical composition

Quantitative chemical analyses were performed using a Shimadzu1720 electron probe microanalyzer at School of Geosciences and Info-Physics, Central South University, China. The following experimental conditions were used: wavelength-dispersive spectroscopy mode, accelerating voltage = 15 kV, beam current = 10 nA, and beam diameter = 1 μm. The standards used were jadeite (Na), magnetite (Fe), rhodonite (Mn), quartz (Si), anorthite (Ca), zircon (Zr), rutile (Ti), fluorite (F). Electron microprobe analysis data (average of 7 spot analyses) are given in Table 2. The empirical formula is calculated on the basis of

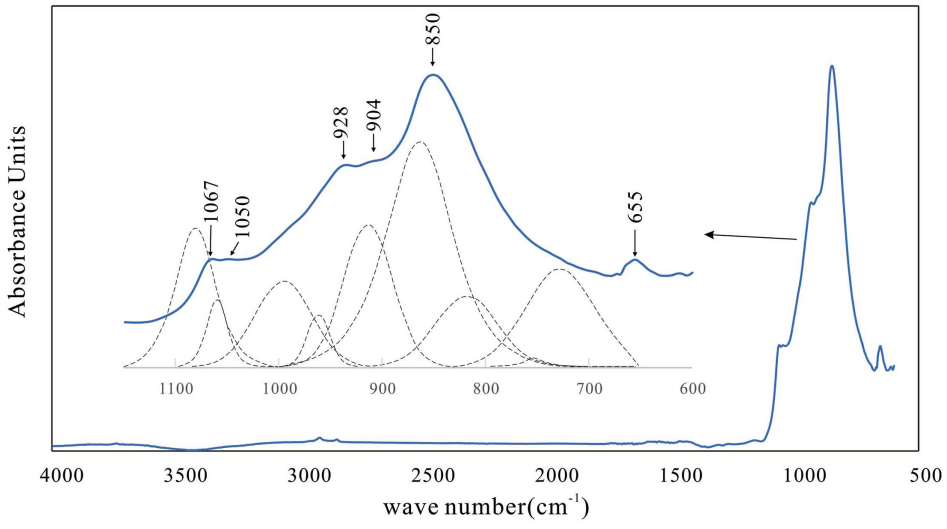

Figure 5. Infrared spectrum of moxuanxueite, compared with the data of normandite from Partomchorr deposit, Kola Peninsula, Russia (Frost et al. 2015).

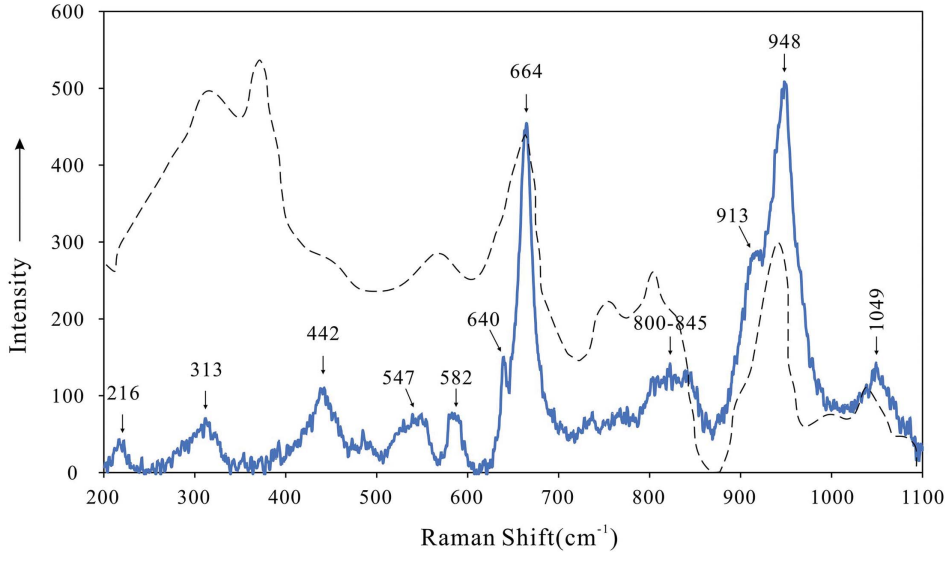

Figure 6. Raman spectrum of moxuanxueite, compared with the data of Zr-rich cuspidine from Pian di Celle, Italy (Sharygin et al. 1996a).

Table 2. Chemical data (wt%) for moxuanxueite

Constituent	Mean	Range	S.D. (σ)	apfu
Na_2O	5.59	5.47–5.77	0.10	1.38
CaO	38.21	37.69–38.98	0.46	5.21
ZrO_2	14.10	13.22–14.70	0.44	0.88
TiO_2	1.42	1.12–1.72	0.21	0.14
FeO	2.12	1.85–2.65	0.27	0.23
MnO	2.03	1.65–2.54	0.28	0.22
SiO_2	31.60	31.08–32.10	0.33	4.03
F	7.82	7.44–8.25	0.27	3.15
F≡O	–3.29			
Total	99.60			

Note: S.D. = standard deviation

O + F = 18 per formula unit. The site-by-site crystal-chemical formula is $Na(Ca_{0.66}Na_{0.38})_{\Sigma 1.04}Ca_4(Ca_{0.55}Fe_{0.23}Mn_{0.22})_{\Sigma 1.00}(Zr_{0.89}Ti_{0.14})_{\Sigma 1.03}(Si_{2.01}O_7)_2(F_{3.15}O_{0.85})_{\Sigma 4.00}$, corresponding to the ideal formula $NaCa_6Zr(Si_2O_7)_2OF_3$, which requires Na_2O 4.06, CaO 44.04, ZrO_2 16.13, SiO_2 31.46, F 7.46, O≡F –3.14, and a total of 100 wt%. Moxuanxueite is chemically similar to hiortdahlite, with only slight differences in the contents of sodium, calcium, and zirconium. The transformation between the two phases is via the following substitution mechanism to maintain charge neutrality: $2Ca^{2+} \leftrightharpoons Na^+ + 0.5Zr^{4+} + 0.5Ca^{2+}$.

X-ray crystallography and structure determination

A light-yellow fragment of moxuanxueite (~100 × 100 × 100 μm) was selected for the X-ray diffraction data collection. Both powder and single-crystal XRD of moxuanxueite were carried out with a Rigaku XtaLAB Synergy diffractometer (Mo*K*α radiation) at School of Geosciences and Info-Physics, Central South University, China. The X-ray powder diffraction data were recorded using Gandolfi technique in powder mode at 50 kV and 1 mA. The pattern was indexed on the basis

Table 3. X-ray powder diffraction data (*d* in Å) for moxuanxueite

I_{meas}	d_{meas}	I_{calc}	d_{calc}	*hkl*
30	**10.42**	**32**	**10.37**	**$\bar{1}$00**
7	5.18	6	5.19	$\bar{2}$00
5	4.87	5	4.88	0$\bar{2}$1
23	**3.280**	**22**	**3.280**	**3 $\bar{1}$0**
100	**3.005**	**100**	**3.008**	**$\bar{1}$12**
57	**2.870**	**56**	**2.870**	**230**
8	2.596	9	2.598	112
26	**2.496**	**29**	**2.504**	**1$\bar{4}$0**
7	2.437	10	2.437	3$\bar{3}$0
10	2.259	12	2.258	1$\bar{4}$2
15	2.033	18	2.034	5 $\bar{1}$0
8	1.964	10	1.963	$\bar{3}$32
32	**1.849**	**30**	**1.847**	**2 $\bar{2}$4**
17	1.803	23	1.804	4$\bar{1}$2
20	**1.701**	**21**	**1.699**	**1$\bar{6}$2**
5	1.631	5	1.631	3 $\bar{6}$3
4	1.602	5	1.601	$\bar{4}$42
8	1.554	9	1.554	$\bar{6}$31
6	1.460	7	1.461	$\bar{7}$ $\bar{3}$1
18	1.417	20	1.418	$\bar{2}$70
5	1.282	5	1.281	$\bar{1}$ 80
2	1.199	3	1.198	$\bar{1}$ 93

Note: The intensities of the seven (7) strongest lines are in bold.

of the calculated pattern based on the unit-cell parameters and the structural model determined by single-crystal XRD using CHEKCELL software (Laugier and Bochu 2004). The refined lattice parameters yielded from the powder XRD data are $a = 11.0286(14)$ Å, $b = 10.9590(13)$ Å, $c = 7.3875(14)$ Å, $\alpha = 109.550(10)°$, $\beta = 109.910(10)°$, $\gamma = 83.360(10)°$, $V = 791.14(10)$ Å^3, $Z = 2$. The seven strongest X-ray powder diffraction lines [*d* in Å (*I*) (*hkl*)] are: 3.005 (100) ($\bar{1}$12), 2.870 (57) (230), 1.849 (32) ($\bar{2}$ $\bar{2}$4), 10.42 (30) ($\bar{1}$00), 2.496 (26) (1$\bar{4}$0), 3.280 (23) (3 $\bar{1}$0), and 1.701 (20) (1$\bar{6}$2). The observed and indexed powder diffraction data for moxuanxueite are listed in Table 3.

The intensity data of single-crystal XRD were corrected for X-ray absorption using the multiscan method, and empirical absorption correction was performed using CrysAlisPro program spherical harmonics (Rigaku Oxford Diffraction 2015), implemented in the SCALE3 ABSPACK scaling algorithm. The refined unit-cell parameters are $a = 11.0235(3)$ Å, $b = 10.9641(4)$ Å, $c = 7.3805(4)$ Å, $\alpha = 109.523(2)°$, $\beta = 109.881(2)°$, $\gamma = 83.434(2)°$, and $V = 790.63(6)$ Å^3; the space group is $P\bar{1}$ (#2). The crystal structure was solved and refined using SHELXT (Sheldrick 2015) and Olex2 software (Dolomanov et al. 2009) starting from the structural model of hiortdahlite given by Bellezza et al. (2012). The following neutral scattering curves, taken from the *International Tables for Crystallography* (Wilson 1992) were used: Ca at Ca1, Ca2, Ca3, and Ca4 sites, Na vs. Ca at Ca5 and Na6 sites, Ca vs. Fe at Ca7 site, Zr vs. Ti at Zr site, Si at Si site, and O vs. F at O7 site. After several cycles of anisotropic refinements for all the atoms, the final anisotropic full-matrix least-squares refinement on F^2 with 746 variables converged at $R_1 = 2.36\%$. The goodness-of-fit was 1.085 (see Online Materials[1] for CIF file). The selected bond distances are provided in Table 4, and the bond-valence sums (BVS) are listed in Table 5. A view of the structure is presented in Figure 7.

Table 4. Selected bond distances (Å) in moxuanxueite

Ca1–O1	2.565(2)	Ca2–O4	2.323(2)
–O2	2.571(2)	–O5	2.480(2)
–O3	2.314(2)	–O6	2.323(2)
–O10	2.634(2)	–O8	2.520(2)
–O11	2.567(2)	–O9	2.337(2)
–O13	2.645(2)	–F2	2.268(1)
–O15	2.489(2)	mean	2.375
–F3	2.268(2)		
mean	2.541		
Ca3–O4	2.351(2)	Ca4–O3	2.331(2)
–O5	2.362(2)	–O4	2.868(2)
–O6	2.364(2)	–O10	2.426(2)
–O8	2.384(2)	–O12	2.390(2)
–O14	2.348(2)	–F1	2.283(1)
–F1	2.278(1)	–F1	2.339(1)
		–F2	2.283(1)
mean	2.348	mean	2.417
Ca5–O2	2.793(3)	Na6–O3	2.609(2)
–O5	2.433(2)	–O6	2.959(2)
–O7	2.412(3)	–O12	2.679(2)
–O9	2.613(2)	–O13	2.392(2)
–O14	2.474(2)	–F1	2.372(2)
–O15	2.925(2)	–F2	2.327(2)
–F3	2.359(2)	–F2	2.271(2)
–F3	2.344(2)		
mean	2.544	mean	2.516
Ca7–O7	2.242(2)	Zr–O7	2.020(2)
–O7′	2.311(3)	–O10	2.095(2)
–O8	2.339(2)	–O11	2.047(2)
–O9	2.290(2)	–O12	2.248(2)
–O14	2.242(2)	–O13	2.090(2)
–F3	2.296(2)	–O15	2.063(2)
mean	2.287	mean	2.094
Si1–O1	1.639(2)	Si2–O1	1.646(2)
–O5	1.614(2)	–O3	1.600(2)
–O12	1.617(2)	–O8	1.609(2)
–O15	1.624(2)	–O11	1.631(2)
mean	1.624	mean	1.622
Si3–O2	1.652(2)	Si4–O2	1.648(2)
–O6	1.594(2)	–O4	1.595(2)
–O13	1.631(2)	–O9	1.600(2)
–O14	1.611(2)	–O10	1.632(2)
mean	1.622	mean	1.619

Discussion

Crystal structure

Moxuanxueite is isostructural with hiortdahlite characterized by two topologically independent polyhedral walls, which distinguish the mineral from the other members of the wöhlerite group (Dal Bo et al. 2022). The ideal compositions of the walls for moxuanxueite could be formed by wall-I: [Zr, Ca, Na, Ca] and wall-II: [Ca, Ca, Ca, Ca]. A schematic view of the cationic distribution in the two kinds of idealized polyhedra walls for moxuanxueite is presented in Figure 8. Both independent walls present a centrosymmetric distribution of cations. The cationic distribution in wall-I of moxuanxueite is topologically and chemically the same as that of hiortdahlite (Dal Bo et al. 2022); Ca1 and Zr polyhedra are in the outer columns, while Na6 and Ca4 polyhedra are in the central columns. The cationic distribution in wall-II of moxuanxueite is similar to cuspidine (different from polyhedral anion coordination); Ca2 and Ca3 polyhedra are in the outer columns, while Ca5 and Ca7 polyhedra are in the central columns. Two diorthosilicate groups link to two edges of the Ca1 polyhedron, while Ca2 and Ca3 polyhedra chelated with one diorthosilicate group on opposite sides (Bellezza et al. 2012).

The Ca1, Ca2, Ca3, and Ca4 sites are completely occupied by calcium cations, whereas the Ca5 and Na6 sites have mixed

Table 5. Bond-valence sum (v.u.) analysis for moxuanxueite

	Ca1	Ca2	Ca3	Ca4	Ca5	Na6	Ca7	Zr	Si1	Si2	Si3	Si4	Sum
O1	0.199								0.960	0.942			2.101
O2	0.195				0.093						0.927	0.937	2.152
O3	0.391			0.374		0.129				1.067			1.961
O4		0.382	0.354	0.088								1.082	1.906
O5		0.250	0.344		0.247				1.027				1.868
O6		0.382	0.342		0.000	0.051					1.084		1.859
O7					0.261		0.376	0.764					1.714
							0.313						
O8		0.224	0.324				0.290			1.041			1.879
O9		0.368			0.152		0.330					1.067	1.917
O10	0.165			0.289				0.624				0.979	2.057
O11	0.198							0.711		0.981			1.890
O12				0.319		0.107		0.413	1.019				1.858
O13	0.160					0.232		0.633			0.981		2.006
O14			0.357		0.221		0.376				1.036		1.990
O15	0.244				0.065			0.680	1.000				1.989
F1			0.308	0.261		0.175							1.048
				0.304									
F2		0.316		0.304		0.197							1.046
						0.229							
F3	0.316				0.215		0.240						0.995
					0.224								
Sum	1.868	1.922	2.029	1.939	1.478	1.120	1.925	3.825	4.006	4.031	4.028	4.065	

Notes: Bond-valence sums were calculated with the site-occupancy factors given in the Online Materials[1] CIF file. Calculations were done using the equation and constants of Brown (1977), $S = \exp[(R_0 - d_0)/b]$.

occupancies by calcium and sodium (the former is a Ca-dominant site, and the latter is a Na-dominant site). Ca1 and Ca5 sites are eightfold coordinated, Ca4 and Na6 sites are sevenfold coordinated, Ca2 and Ca3 sites are sixfold coordinated. The average bond lengths of these independent polyhedral cation sites (in Table 4) are in good agreement with the calculated values for the proposed site occupations on the basis of the effective ionic radii given by Shannon (1976). The Ca7 site (also called *M*-site or *X*7-site in previous literature) was refined with Ca and Fe, representing a scattering factor value of ~22.7 electrons, which compares with the value of ~22.5 electrons derived from electron-microprobe data. The average bond distance of Ca7–O is 2.287 Å, indicating that almost all iron and manganese at the Ca7 site should be bivalent. The mean bond distance (2.287 Å) of Ca7–O in moxuanxueite is longer than those in hiortdahlite [2.235 Å (Merlino and Perchiazzi 1985); 2.231 Å (Dal Bo et al. 2022)], consistent with the fact that the latter is simply occupied by ($Zr_{0.5}Ca_{0.5}$) at the *X*7 (Ca7) site (Dal Bo et al. 2022). The Zr site

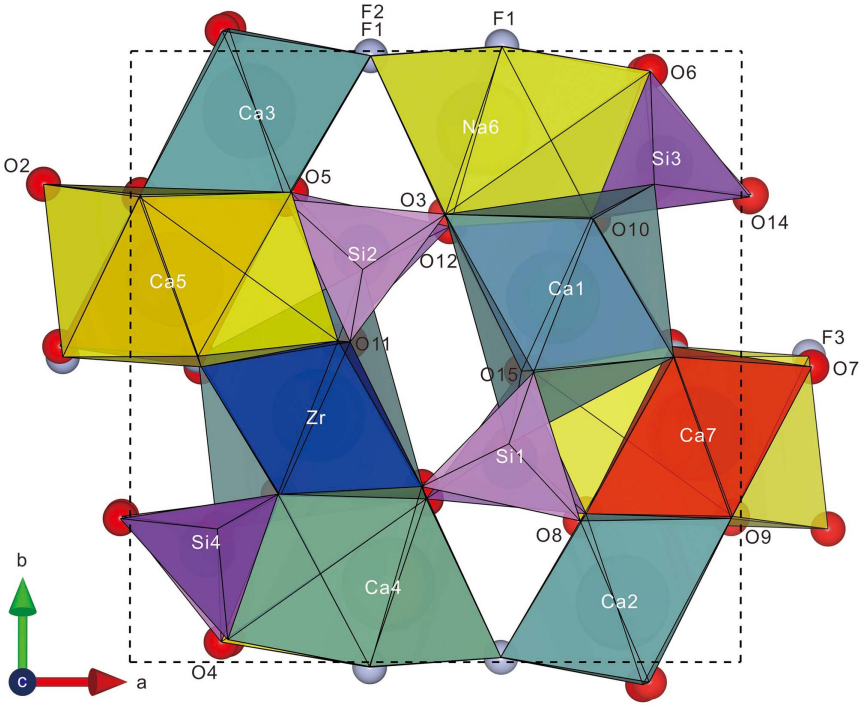

Figure 7. Crystal structure of moxuanxueite, drawn using the Vesta software (Momma and Izumi 2011).

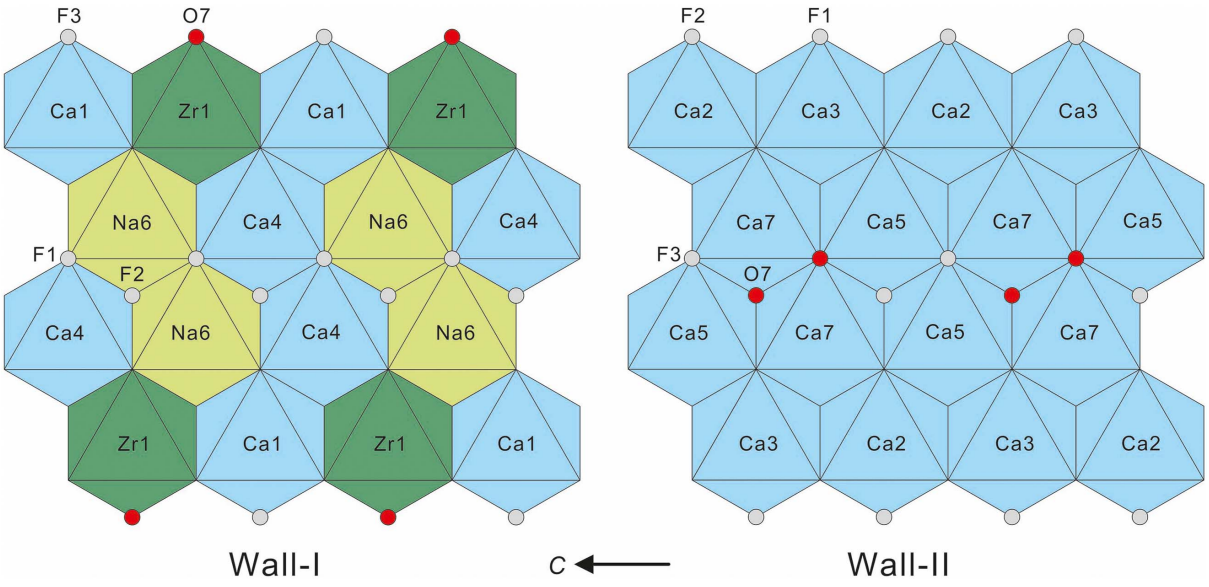

Figure 8. Schematic view of the cationic distribution in the idealized polyhedra walls of moxuanxueite (drawn as octahedra to obtain a clearer view of the structure).

is occupied by zirconium with minor substitution of titanium for zirconium, with an average bond length of 2.094 Å, which is consistent with the reported Zr–O distances of the hiortdahlite-type materials (Table 6) (Merlino and Perchiazzi 1985; Bellezza et al. 2012; Biagioni et al. 2012; Dal Bo et al. 2022).

The bond valences (v.u.) of moxuanxueite were calculated using the bond-valence parameters of Brown and Altermatt (1985). The BVS calculated for Si sites, 4.006, 4.031, 4.028, and 4.065, are within error of the same as the ideal values. The BVS for the Ca1, Ca2, Ca3, Ca4, Ca5 site, Na6 site, Ca7 site, and Zr site are 1.868, 1.922, 2.029, 1.939, 1.478, 1.120, 1.925, and 3.825 v.u., respectively, which agrees with their refined occupancies. The BVS for the Ca7-site showed that it is dominated by divalent cations, which is different from hiortdahlite, which is dominated by mixed trivalent cations (Merlino and Perchiazzi 1985). This is a significant difference between hiortdahlite and moxuanxueite; for this reason, a redefinition of hiortdahlite has been approved by the IMA-CNMNC in 2020 [Proposal 20-D (Miyawaki et al. 2020)]. The ideal formula of hiortdahlite has been revised to $Na_2Ca_4(Ca_{0.5}Zr_{0.5})Zr(Si_2O_7)_2OF_3$, with a valency-imposed mixed site-occupancy at the Ca7 (also called *X*7 or *M*) site (Dal Bo et al. 2022). The BVS for the O1–O15 sites of moxuanxueite are 2.101, 2.152, 1.961, 1.906, 1.868, 1.859, 1.714, 1.879, 1.917, 2.057, 1.890, 1.858, 2.006, 1.990, and 1.989 v.u., respectively. The lower sum of the valences for the O7 site suggests that it is a mixed occupancy by oxygen and

Table 6. Comparative characteristics of moxuanxueite and other similar species in wöhlerite group

	Moxuanxueite	*Hiortdahlite I*[a]	*Hiortdahlite I*[b]
Ideal formula	**$NaCa_6Zr(Si_2O_7)_2OF_3$**	**$Na_2Ca_4Zr(Zr_{0.5}Ca_{0.5})(Si_2O_7)_2OF_3$**	**$NaCa_6Zr(Si_2O_7)_2OF_3$**
Crystal system	triclinic	triclinic	triclinic
Space group	$P\bar{1}$	$P\bar{1}$	$P\bar{1}$
a (Å)	11.0235(3)	11.0149(9)	10.991(7)
b (Å)	10.9641(4)	10.9409(9)	10.934(3)
c (Å)	7.3805(4)	7.3534(3)	7.366(2)
α (°)	109.523(2)	109.350(3)	109.60(3)
β (°)	109.881(2)	109.879(4)	109.43(2)
γ (°)	83.434(2)	83.434(4)	83.55(3)
V (Å^3)	790.63(6)	786.30(8)	786.4(6)
CaNa5 site	$Ca_{0.64}Na_{0.36}$	$Na_{0.6}Ca_{0.4}$	$Ca_{0.65}Na_{0.35}$
NaCa6 site	$Na_{0.74}Ca_{0.26}$	Na	$Na_{0.95}REE_{0.05}$
M (Ca7) site	$Ca_{0.55}Fe_{0.45}$	$Zr_{1/3}Ti_{1/6}Ca_{1/6}Mn_{1/6}Fe_{1/6}$	$Ca_{0.44}Mn_{0.29}Fe_{0.15}Ti_{0.07}Mg_{0.05}$
Zr site	$Zr_{0.85}Ti_{0.15}$	Zr	$Zr_{0.90}Nb_{0.05}Ti_{0.05}$
Ca1–O (Å)	2.541	2.524	2.50
Ca2–O (Å)	2.375	2.380	2.36
Ca3–O (Å)	2.348	2.346	2.34
Ca4–O (Å)	2.417	2.418	2.43
CaNa5–O (Å)	2.554	2.569	2.54
NaCa6–O (Å)	$^{[VI]}$2.444 ($^{[VII]}$2.554)	$^{[VI]}$2.433	$^{[VII]}$2.51
M–O (Å)	2.287	2.235	2.26
Zr–O (Å)	2.094	2.090	2.11

[a] Data from Merlino and Perchiazzi (1985).
[b] Data from Biagioni et al. (2012).

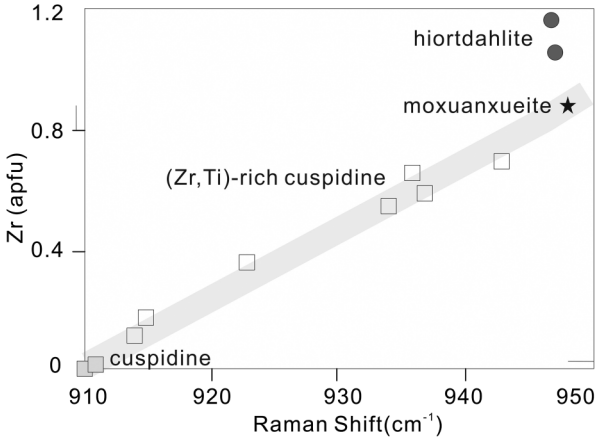

Figure 9. Plot of Si-O stretching vibration (cm^{-1}) vs. Zr (apfu) for wöhlerite-group minerals (after Sharygin et al. 1996a).

fluorine. The bond-valence sums for the F1, F2, and F3 sites are 1.048, 1.046, and 0.995 v.u., respectively. As shown in Table 5, all the BVS results are in agreement with the ideal values, and the model satisfies the charge-balance requirement.

Previous findings of moxuanxueite analog minerals

Despite that moxuanxueite was approved recently, several occurrences of moxuanxueite analog minerals have been previously reported. Sharygin et al. (1996a) investigated a series of Zr-Ti disilicates from Pian di Celle in Italy and found a special mineral phase (named Zr-rich cuspidine) with a high Zr content of up to 10.46%. The component of this Zr-rich cuspidine phase corresponds to the ideal formula, $NaCa_6Zr(Si_2O_7)_2OF_3$. Furthermore, as noted by these authors, the XRD pattern of this mineral indicates that it belongs to the cuspidine group and is more like hiortdahlite. This is also consistent with the characteristics of their Raman spectrum. Compared with the strongest peak of cuspidine at 910 cm^{-1}, the main peak around 950 cm^{-1} of the Zr-rich cuspidine phase is closer to that of hiortdahlite. The authors also reported a relationship between Si-O stretching vibration and the Zr content; our Raman spectroscopic result is consistent with this trend, i.e., the shift of the Raman main peak is positively correlated with the Zr content (Fig. 9). The medium-intensity peaks around 750–850 cm^{-1} are attributed to the substitution of F for O, which is commonly observed in hiortdahlite but absent in cuspidine. These lines of evidence indicate that the Zr-rich cuspidine phase from Pian di Celle in Italy should be the same mineral phase as moxuanxueite. The combined substitution of $4Ca^{2+} + F^- \leftrightharpoons 2Na^+ + 1.5Zr^{4+} + 0.5Ca^{2+} + O^{2-} \leftrightharpoons Na^+ + Zr^{4+} + 2Ca^{2+} + O^{2-}$ is the main mechanism of chemical variation among cuspidine, hiortdahlite, and moxuanxueite.

Another occurrence of the Ca-dominant *M*-site hiortdahlite was reported from the Los Archipelago, Guinea (Biagioni et al. 2012). The hiortdahlite-*I* mineral has a low BVS (2.14 v.u.) of the mixed occupancy *M*-site ($Ca_{0.44}Mn_{0.29}Fe_{0.15}Ti_{0.07}Mg_{0.05}$), which is significantly different from 3 v.u. of the *M*-site ($Ca_{0.5}Zr_{0.5}$) in hiortdahlite. In addition, this mineral has a Ca-dominant NaCa site, which is the same as moxuanxueite but different from hiortdahlite (Table 6). Although there are over 4 apfu of F in the empirical formula calculated from EMPA data, the relatively high BVS value (1.52 v.u.) of O7 indicates a mixed (O, F) occupancy at the O7 site (Biagioni et al. 2012). Considering the EMPA accuracy of F contents and the high-quality structural data from single-crystal XRD, this mineral is probably the same as moxuanxueite. It is notable that both hiortdahlite-I and the domain IV phase of guanirite from Monte Somma, Italy (Bellezza et al. 2012) have high manganese contents. For some Mn-rich points analyzed by EMPA, Mn is probably very close to the dominant Ca constituent of the *M*-site. Hence, it is logical to infer that the Mn end-member of moxuanxueite may exist in nature.

Genesis of moxuanxueite

Peralkaline igneous rocks host deposits of HFSE, as well as rare earth elements (REE), which represent one of the most potentially economically important resources for critical metals (Dostal 2017; Yang et al. 2024). Compared with zircon, which is the main zirconium-containing mineral in most granites, zirconium in agpaitic rocks is mainly hosted in complex Na-Ca-Zr-disilicate minerals, i.e., wöhlerite, eudialyte, and rinkite group minerals (Chakhmouradian and Mitchell 2002; Pekov 2000, 2005; Andersen et al. 2010, 2013; Kynicky et al. 2011; Chukanov et al. 2014; Marks and Markl 2017).

Previous studies suggest that wöhlerite is an unambiguous early liquidus mineral (Sunde et al. 2018), which is consistent with the microscopic observation that moxuanxueite is a primary crystallization phase in the Gejiu alkaline complex. The study of the solubility of wöhlerite in SiO_2-undersaturated melts shows that wöhlerite is a primary mineral in the early crystallization sequence of the magmatic system and could be stable up to high temperatures (ranging from 750 to 1000 °C) (Schmidt et al. 2023). This is consistent with the calculated temperatures of magma crystallization of Gejiu alkaline complex (697–896 °C, mean 801 °C) (Wang et al. 2019). It is worth noting that moxuanxueite is closely related to sodalite, as well as other halogen-bearing minerals, e.g., fluorbritholite-(Ce), fluorcalciobritholite, and fluorapatite. This mineral assemblage is consistent with the observations of hiortdahlite (e.g., Marks and Markl 2017 and references therein). Previous experimental study by Giehl et al. (2014) indicates that high melt concentrations of Cl and F could stabilize the formation of hiortdahlite and other halogen-bearing mineral phases such as fluorite, sodalite, and eudialyte. Accordingly, the stable assemblage of zircon and fluorite shifts to the F-rich Zr-Ti disilicates (e.g., wöhlerite and rinkite group minerals) and fluorite, which commonly indicates that a_{HF} increases to a high level in a magma (Andersen et al. 2010; Giehl et al. 2014).

The primary alteration products of moxuanxueite are mainly hydrous zirconosilicate, including catapleiite, bobtraillite, and eudialyte group minerals (Wang et al. 2023a, 2023b). These observations can be compared to those in the nepheline syenite pegmatites from the Langesundsfjord archipelago, Norway (Andersen et al. 2010), illustrating the contribution of water participating in the dissolution-reprecipitation of HFSE and other rare elements during the late-magmatic hydrothermal process in a relatively low temperature environment (400–348 °C) (Kynicky et al. 2011; Chakrabarty et al. 2016).

Implications

Moxuanxueite is a new Zr-disilicate discovered in the Gejiu alkaline complex. It was formed early in the crystallization process of the magmatic system with high Cl and F concentrations at a high temperature of about 800 °C. Moxuanxueite offers important insights into the chemical variability of wöhlerite-group minerals. Furthermore, the abundant distribution of critical metal-bearing minerals, such as Zr-Nb-Ti disilicates, REE carbonates, and Li-B-bearing mineral assemblages in the Gejiu alkaline complex is very similar to those in other well-known alkaline complexes such as the Mont Saint-Hilaire (Canada), Ilímaussaq (Greenland), Langesundsfjord (Norway), and Saima (China). In spite of the fact that agpaitic rocks are relatively rare worldwide, they act as an important carrier for HFSEs from the deep mantle to the shallow crust. From this point of view, moxuanxueite, as well as other wöhlerite group species, as the common accessory Zr-Nb-Ti-bearing minerals, are not only important in understanding the crust-mantle cycle of HFSE elements but are also of economic interest as a promising source of critical metals.

Acknowledgments and Funding

The authors thank Hexiong Yang for his valuable suggestions on the structure refinement issues. We acknowledge CNMNC members for their insights on the new mineral proposal, especially Fabrice Dal Bo is thanked for the discussion on the ideal formula of moxuanxueite. The authors are grateful to M. Santosh for the improvement of language quality. We gratefully acknowledge Yinhang Cheng, Ruoshi Jin, Xiaoming Sun, and Fengqing Zhao for their precious help and support in discovering the new mineral species. We also sincerely thank the three anonymous reviewers and Associate Editor Aaron J. Lussier for their constructive comments and suggestions, which greatly improved the quality of this manuscript. This study was financially supported by the Scientific Innovation Program (202303AA08000601, 2023XAGG0068), the National Natural Science Foundation of China (NSFC) (92062217, 41502033, 42072054), the China Geological Survey Project (DD20160129-03), and the China Scholarship Council (CSC) (202106400047, 202108575009).

References Cited

Al-Hermezi, H.M., McKie, D., and Hall, A.J. (1986) Baghdadite, a new calcium zirconium silicate mineral from Iraq. Mineralogical Magazine, 50, 119–123, https://doi.org/10.1180/minmag.1986.050.355.15.

Andersen, T., Erambert, M., Larsen, A.O., and Selbekk, R.S. (2010) Petrology of nepheline syenite pegmatites in the Oslo Rift, Norway: Zirconium silicate mineral assemblages as indicators of alkalinity and volatile fugacity in mildly agpaitic magma. Journal of Petrology, 51, 2303–2325, https://doi.org/10.1093/petrology/egq058.

——— (2013) Petrology of nepheline syenite pegmatites in the Oslo Rift, Norway: Zr and Ti mineral assemblages in miaskitic and agpaitic pegmatites in the Larvik Plutonic Complex. Mineralogia, 44, 61–98, https://doi.org/10.2478/mipo-2013-0007.

Bellezza, M., Merlino, S., and Perchiazzi, N. (2004) Chemical and structural study of the Zr, Ti-disilicates in the venanzite from Pian di Celle, Umbria, Italy. European Journal of Mineralogy, 16, 957–969, https://doi.org/10.1127/0935-1221/2004/0016-0957.

——— (2012) Distinct domains in "guarinite" from Monte Somma, Italy: Crystal structures and crystal chemistry. Canadian Mineralogist, 50, 531–548, https://doi.org/10.3749/canmin.50.2.531.

Biagioni, C., Merlino, S., Parodi, G.C., and Perchiazzi, N. (2012) Crystal chemistry of minerals of the wöhlerite group from the Los Archipelago, Guinea. Canadian Mineralogist, 50, 593–609, https://doi.org/10.3749/canmin.50.3.593.

Brown, I.D. (1977) Predicting bond lengths in inorganic crystals. Acta Crystallographica Section B, 33, 1305–1310, https://doi.org/10.1107/S0567740877005998.

Brown, I.D. and Altermatt, D. (1985) Bond-valence parameters obtained from a systematic analysis of the Inorganic Crystal Structure Database. Acta Crystallographica Section B, 41, 244–247, https://doi.org/10.1107/S0108768185002063.

Chakhmouradian, A.R. (2006) High-field-strength elements in carbonatitic rocks: Geochemistry, crystal chemistry and significance for constraining the sources of carbonatites. Chemical Geology, 235, 138–160, https://doi.org/10.1016/j.chemgeo.2006.06.008.

Chakhmouradian, A.R. and Mitchell, R.H. (2002) The mineralogy of Ba-and Zr-rich alkaline pegmatites from Gordon Butte, Crazy Mountains (Montana, USA): Comparisons between potassic and sodic agpaitic pegmatites. Contributions to Mineralogy and Petrology, 143, 93–114, https://doi.org/10.1007/s00410-001-0333-6.

Chakhmouradian, A.R. and Williams, C.T. (2004) Mineralogy of high-field-strength elements (Ti, Nb, Zr, Ta, Hf) in phoscoritic and carbonatitic rocks of the Kola Peninsula, Russia. In F. Wall and A.N. Zaitsev, Eds., Phoscorites and Carbonatites from Mantle to Mine: The Key Example of the Kola Alkaline Province, p. 293–340. Mineralogical Society of Great Britain and Ireland.

Chakrabarty, A., Mitchell, R.H., Ren, M., Saha, P.K., Pal, S., Pruseth, K.L., and Sen, A.K. (2016) Magmatic, hydrothermal and subsolidus evolution of the agpaitic nepheline syenites of the Sushina Hill Complex, India: Implications for the metamorphism of peralkaline syenites. Mineralogical Magazine, 80, 1161–1193, https://doi.org/10.1180/minmag.2016.080.057.

Chao, G.Y. and Gault, R.A. (1997) Normandite, the Ti-analogue of låvenite from Mont Saint-Hilaire, Quebec. Canadian Mineralogist, 35, 1035–1039.

Chen, W. (2019) The granitic magmatism and its significance of mineralization in Gejiu, Yunnan, 63 p. Master's thesis, China University of Geosciences (Beijing) (in Chinese with English abstract).

Chen, X.Y., Wang, Y.J., Zhang, Y.Z., Zhang, A.M., and Cao, Y.J. (2013) Geochronology and geochemical characteristics of the Nandu syenite in SE Guangxi and its implications. Geotectonica et Metallogenia, 37, 284–293 (in Chinese with English abstract).

Cheng, Y.B. (2012) Spatial-temporal evolution of the magmatism and mineralization in the Gejiu supergiant Sn polymetallic district and insights into serval key problems, 340 p. Ph.D. thesis, China University of Geosciences (Beijing) (in Chinese with English abstract).

Cheng, Y.B. and Mao, J.W. (2010) Age and geochemistry of granites in Gejiu area, Yunnan province, SW China: Constraints on their petrogenesis and tectonic setting. Lithos, 120, 258–276, https://doi.org/10.1016/j.lithos.2010.08.013.

Cheng, Y.B., Mao, J.W., Chen, M.H., Yang, Z.X., Feng, J.R., and Zhao, H.J. (2008) LA-ICP-MS zircon dating of the alkaline rocks and lamprophyres in Gejiu area and its implications. Geology in China, 35, 1138–1149 (in Chinese with English abstract).

Cheng, Y.B., Mao, J.W., Xie, G.Q., Chen, M.H., and Yang, Z.X. (2009) Zircon U-Pb dating of granites in Gejiu superlarge tin polymetallic orefield and its significance. Mineralium Deposita, 28, 297–312 (in Chinese with English abstract).

Cheng, Y.B., Mao, J.W., and Spandler, C. (2013) Petrogenesis and geodynamic implications of the Gejiu igneous complex in the western Cathaysia block, South China. Lithos, 175-176, 213–229, https://doi.org/10.1016/j.lithos.2013.04.002.

Chukanov, N.V. (2014) Infrared spectra of mineral species: Extended library, p. 1025–1026. Springer Geochemistry/Mineralogy.

Chukanov, N.V., Krivovichev, S.V., Pakhomova, A.S., Pekov, I.V., Schäfer, C., Vigasina, M.F., and Van, K.V. (2014) Laachite, $(Ca,Mn)_2Zr_2Nb_2TiFeO_{14}$, a new zirconolite-related mineral from the Eifel volcanic region, Germany. European Journal of Mineralogy, 26, 103–111, https://doi.org/10.1127/0935-1221/2013/0025-2343.

Dal Bo, F., Friis, H., and Mills, S.J. (2022) Nomenclature of wöhlerite-group minerals. Mineralogical Magazine, 86, 661–676, https://doi.org/10.1180/mgm.2022.10.

Dal Bo, F., Friis, H., Elburg, M.A., Hatert, F., and Andersen, T. (2024) Pilanesbergite: A new rock-forming mineral occurring in nepheline syenite from the Pilanesberg Alkaline Complex, South Africa. European Journal of Mineralogy, 36, 73–85, https://doi.org/10.5194/ejm-36-73-2024.

Dolomanov, O.V., Bourhis, L.J., Gildea, R.J., Howard, J.A.K., and Puschmann, H. (2009) A complete structure solution, refinement and analysis program. Journal of Applied Crystallography, 42, 339–341, https://doi.org/10.1107/S0021889808042726.

Dostal, J. (2017) Rare earth element deposits of alkaline igneous rocks. Resources, 6, 34, https://doi.org/10.3390/resources6030034.

Du, Y.S., Huang, H.W., Huang, Z.Q., Xu, Y.J., Yang, J.H., and Huang, H. (2009) Basin translation from Late Palaeozoic to Triassic of Youjiang Basin and its tectonic significance. Geological Science and Technology Information, 28, 10–15 (in Chinese with English abstract).

Frost, R.L., López, A., Theiss, F.L., Scholz, R., and Romano, A.W. (2015) A vibrational spectroscopic study of the silicate mineral normandite-NaCa(Mn^{2+}, Fe^{2+})(Ti,Nb,Zr)Si_2O_7(O,F)$_2$. Spectrochimica Acta Part A: Molecular and Biomolecular Spectroscopy, 135, 801–804, https://doi.org/10.1016/j.saa.2014.07.035.

Galuskin, E., Pertsev, N., Armbruster, T., Kadiyski, M., Zadov, A., Galuskina, I., Dzier anowski, P., Wrzalik, R., and Kislov, E. (2007) Dovyrenite $Ca_6Zr[Si_2O_7]_2(OH)_4$—A new mineral from skarned carbonate xenoliths in basic-ultrabasic rocks of the Ioko-Dovyren Massif, Northern Baikal Region, Russia. Mineralogia, 38, 15–28, https://doi.org/10.2478/v10002-007-0012-y.

Giehl, C., Marks, M.A., and Nowak, M. (2014) An experimental study on the influence of fluorine and chlorine on phase relations in peralkaline phonolitic melts. Contributions to Mineralogy and Petrology, 167, 977, https://doi.org/10.1007/s00410-014-0977-7.

Huang, W.L., Xu, J.F., Chen, J.L., Huang, F., Zeng, Y.C., Pi, Q.H., Cai, Y.F., and Jiang, X.Z. (2016) Geochronology and geochemistry of the Gejiu complex in the Yunnan Province, SW China: Petrogenesis and contributions of mantle-derived melts to tin mineralization. Yanshi Xuebao, 32, 2330–2346 (in Chinese with English abstract).

Kynicky, J., Chakhmouradian, A.R., Xu, C., Krmicek, L., and Galiova, M. (2011) Distribution and evolution of zirconium mineralization in peralkaline granites and associated pegmatites of the Khan Bogd complex, southern Mongolia. Canadian Mineralogist, 49, 947–965, https://doi.org/10.3749/canmin.49.4.947.

Laugier, J. and Bochu, B. (2004) LMGP Suite of Programs for the Interpretation of X-ray Experiments. ENSP/Laboratoire des Matériaux et du Génie Physique.

Mandarino, J.A. (1981) The Gladstone-Dale relationship: Part 4. The compatibility concept and its application. Canadian Mineralogist, 19, 441–450.

Mariano, A.N. and Roeder, P.L. (1989) Wöhlerite: Chemical composition, cathodoluminescence and environment of crystallization. Canadian Mineralogist, 27, 709–720.

Marks, M.A. and Markl, G. (2017) A global review on agpaitic rocks. Earth-Science Reviews, 173, 229–258, https://doi.org/10.1016/j.earscirev.2017.06.002.

Mellini, M. (1981) Refinement of the crystal structure of låvenite. Tschermak's Mineralogische und Petrographische Mitteilungen, 28, 99–112, https://doi.org/10.1007/BF01081548.

——— (1982) Niocalite revised: Twinning and crystal structure. Tschermak's Mineralogische und Petrographische Mitteilungen, 30, 249–266, https://doi.org/10.1007/BF01087171.

Mellini, M. and Merlino, S. (1979) Refinement of the crystal structure of wöhlerite. Mineralogy and Petrology, 26, 109–123, https://doi.org/10.1007/BF01081296.

Merlino, S. and Perchiazzi, N. (1985) The crystal structure of hiortdahlite I. Tschermak's Mineralogische und Petrographische Mitteilungen, 34, 297–310, https://doi.org/10.1007/BF01082969.

——— (1988) Modular mineralogy in the cuspidine group of minerals. Canadian Mineralogist, 26, 933–943.

Merlino, S., Perchiazzi, N., Khomyakov, A.P., Pushcharovskii, D.Y., Kulikova, I.M., and Kuzmin, V.I. (1990) Burpalite, a new mineral from Burpalinskii massif, North Transbajkal, USSR: Its crystal structure and OD character. European Journal of Mineralogy, 2, 177–186, https://doi.org/10.1127/ejm/2/2/0177.

Mills, S.J., Dal Bo, F., Alves, P., Friis, H., and Missen, O.P. (2022) Madeiraite, IMA 2021-077. CNMNC Newsletter 64. Mineralogical Magazine, 86, 178–182.

Miyawaki, R., Hatert, F., Pasero, M., and Mills, S.J. (2020) IMA Commission on New Minerals, Nomenclature and Classification (CNMNC) Newsletter 57. Mineralogical Magazine, 84, 791–794, https://doi.org/10.1180/mgm.2020.73.

Momma, K. and Izumi, F. (2011) VESTA 3 for three-dimensional visualization of crystal, volumetric and morphology data. Journal of Applied Crystallography, 44, 1272–1276, https://doi.org/10.1107/S0021889811038970.

Pekov, I.V. (2000) Lovozero Massif: History, Pegmatites, Minerals, 484 p. Ocean Pictures Ltd.

——— (2005) Genetic mineralogy and crystal chemistry of rare elements in highly alkaline postmagmatic systems. Ph.D. thesis, Moscow State University, Russia (in Russian).

Raade, G. and Mladeck, M.H. (1983) Janhaugite, $Na_3Mn_3Ti_2Si_4O_{15}(OH,F,O)_3$, a new mineral from Norway. American Mineralogist, 68, 1216–1219.

Rigaku Oxford Diffraction (2015) CrysAlisPro Software system, version 1.171.38.43. Rigaku Corporation.

Saburi, S., Kawahara, A., Henmi, C., Kusachi, I., and Kihara, K. (1977) The refinement of the crystal structure of cuspidine. Mineralogical Journal, 8, 286–298, https://doi.org/10.2465/minerj.8.286.

Schmidt, C., Nikolenko, A., Appelt, O., Gottsche, A., Sieber, M., Veksler, I., and Sunde, Ø. (2023) Chemical controls on niobium and zirconium mobility inferred from dissolution experiments on wöhlerite in alkaline silica-undersaturated melts. Chemical Geology, 621, 121370, https://doi.org/10.1016/j.chemgeo.2023.121370.

Shang, Z. (2017) Zircon U-Pb geochronology, geochemistry and implication for tectonic setting of Jiasha complex in Gejiu district. Master's dissertation, China University of Geosciences (Beijing), 1–62 (in Chinese with English abstract).

Shannon, R.D. (1976) Revised effective ionic radii and systematic studies of interatomic distances in halides and chalcogenides. Acta Crystallographica Section A, 32, 751–767, https://doi.org/10.1107/S0567739476001551.

Sharygin, V.V., Stoppa, F., and Kolesov, B.A. (1996a) Zr-Ti disilicates from the Pian di Celle volcano, Umbria, Italy. European Journal of Mineralogy, 8, 1199–1212, https://doi.org/10.1127/ejm/8/5/1199.

——— (1996b) Cuspidine in melilitolites of San Venanzo, Italy. Transactions of the Russian Academy of Sciences. Earth Science Sections, 349, 747–751.

Sheldrick, G.M. (2015) Crystal structure refinement with SHELXL. Acta Crystallographica Section C, 71, 3–8, https://doi.org/10.1107/S2053229614024218.

Sunde, Ø., Friis, H., and Andersen, T. (2018) Variation in major and trace elements of primary wöhlerite as an indicator of the origin of Pegmatites in the Larvik plutonic complex, Norway. Canadian Mineralogist, 56, 529–542, https://doi.org/10.3749/canmin.1700050.

Wang, X.Z. (2006) Research on the geological and geochemical features and the petrogenesis of Gejiu complex, Yunnan province, 76 p. Master's thesis, Institute of Geochemistry, Chinese Academic of Science (in Chinese with English abstract).

Wang, Y., Dong, G., Chen, W., Su, L., Yin, G., Zhu, H., and Li, H. (2019) Characteristics and petrogenesis of feldspathoid syenite in Gejiu, Yunnan. Earth Science Frontiers, 26, 209–220 (in Chinese with English abstract).

Wang, Y., Dong, G., Santosh, M., Liu, C., Chen, W., Liang, J., and Zhang, Y. (2021) Alkaline magmatism on Neo-Tethyan extensional domains: Evidences from the Gejiu complex in Yunnan, China. Geological Journal, 56, 4331–4348, https://doi.org/10.1002/gj.4165.

Wang, Y., Nestola, F., Hou, Z., Gu, X., Dong, G., Yang, Z., Fan, G., Xiao, Z., and Qu, K. (2023a) Bobtraillite from Gejiu hyperagpaitic nepheline syenite, southwestern China: New occurrence and crystal structure. European Journal of Mineralogy, 35, 65–74, https://doi.org/10.5194/ejm-35-65-2023.

Wang, Y., Gu, X., Dong, G., Hou, Z., Nestola, F., Yang, Z., Fan, G., Wang, Y., and Qu, K. (2023b) Calcioancylite-(La), $(La,Ca)_2(CO_3)_2(OH,H_2O)_2$, a new member of the ancylite group from Gejiu nepheline syenite, Yunnan Province, China. Mineralogical Magazine, 87, 554–560, https://doi.org/10.1180/mgm.2023.28.

Warr, L.N. (2021) IMA–CNMNC approved mineral symbols. Mineralogical Magazine, 85, 291–320, https://doi.org/10.1180/mgm.2021.43.

Wilson, A.J.C. (1992) International Tables for Crystallography. Volume C. Kluwer, Dordrecht.

Yang, W.B., Niu, H.C., Li, N.B., Hollings, P., Zurevinski, S., and Mitchell, R.H. (2024) Scavenging and release of REE and HFSE by Na-metasomatism in magmatic-hydrothermal systems. Fundamental Research (Beijing), 4, 315–323, https://doi.org/10.1016/j.fmre.2022.04.004.

Yu, Y.R. (1993) REE characteristics of alkaline rock body in Baiyunshan, Gejiu. Yunnan Geology, 3, 277–289 (in Chinese with English abstract).

Zhang, Y., Huang, Z.L., Luo, T.Y., Qian, Z.K., Zhang, J.W., and Sun, J.B. (2013) The geochemistry and SIMS U-Pb zircon dating of the Jiasha gabbric-monzonitic intrusion in Gejiu district, Yunnan Province. Geochimica, 42, 523–543 (in Chinese with English abstract).

Zhao, Z., Qi, L., Huang, Z.L., Yan, Z.F., and Xu, C. (2012) Trace elements and Sr-Nd isotopic geochemistry and genesis of Jijiealkaline-ultramafic rocks, southern part of Panxi rift. Yanshi Xuebao, 28, 1915–1927 (in Chinese with English abstract).

Zhao, J.N., Zuo, R.G., Chen, S.Y., and Kreuzer, O.P. (2015) Application of the tectono-geochemistry method to mineral prospectivity mapping: A case study of the Gaosong tin-polymetallic deposit, Gejiu district, SW China. Ore Geology Reviews, 71, 719–734, https://doi.org/10.1016/j.oregeorev.2014.09.023.

Manuscript received March 20, 2024
Manuscript accepted January 16, 2025
Accepted manuscript online January 29, 2025
Manuscript Handled by Aaron J. Lussier

Endnotes:

[1]Deposit item AM-25-109397. Online Materials are free to all readers. Go online, via the table of contents or article view, and find the tab or link for supplemental materials. The CIF has been peer-reviewed by our Technical Editors.